Atmospheric winter response to Arctic sea ice changes in reanalysis data and model simulations

Ralf Jaiser[1], Tetsu Nakamura[2,3], Dörthe Handorf[1], Klaus Dethloff[1], Jinro Ukita[4], Koji Yamazaki[2,3]

[1]Alfred-Wegener-Institut, Helmholtz-Zentrum für Polar- und Meeresforschung, Potsdam, Germany.

[2]National Institute of Polar Research, Tachikawa, Japan.

[3]Hokkaido University, Sapporo, Japan.

[4]Niigata University, Niigata, Japan

Corresponding author: Ralf Jaiser (ralf.jaiser@awi.de)

Key Points:

- Simulation of Arctic sea ice impact shows high resemblance to observed stratosphere-troposphere coupling in time and space
- Significant connection with the stratosphere first appears in Barents and Kara Sea region and subsequently in Pacific region
- Stratospheric response to sea ice changes is robust regardless of decadal scale variations of SSW occurrence

Abstract

The changes of atmospheric flow patterns related to Arctic Amplification have impacts well beyond the Arctic regional weather and climate system. Here we examine modulations of vertically propagating planetary waves, a major feature of the climate response to Arctic sea ice reduction by comparing the corresponding results of an atmospheric general circulation model with reanalysis data for periods of high and low sea ice conditions. Under low sea ice condition we find enhanced coupling between troposphere and stratosphere starting in November with preferred polar stratospheric vortex breakdowns in February, which then feeds back to the troposphere. The model experiment and ERA-Interim reanalysis data agree well with respect to temporal and spatial characteristics associated with vertical planetary wave propagation including its precursors. The upward propagating planetary wave anomalies resemble a wave number 1 and 2 pattern depending on region and timing. Since our experimental design only allows influences from sea ice changes and there is a high degree of resemblance between model results and observations, we conclude that sea ice is a main driver of observed winter circulation changes.

1 Introduction

In recent years the Arctic is undergoing substantial changes with stronger positive temperature trends than anywhere else, widely known as Arctic Amplification [*Alexeev et al.*, 2012]. Increasing temperatures are tightly connected to sea ice cover reduction through the ice-albedo feedback [*Stroeve et al.*, 2012]. Additionally clouds and water vapor have amplifying effects on the Arctic warming throughout the year [*Taylor et al.*, 2013; *Pithan and Mauritsen*, 2014]. The surface based warming affects Arctic weather systems. Increased heat fluxes and reduced vertical stability lead to enhanced baroclinic systems [*Jaiser et al.*, 2012], which result in more frequent and more intense Arctic synoptic cyclones in autumn [*Stroeve et al.*, 2012].

Arctic changes have remote influences via multiple mechanisms and processes [*Vihma*, 2014]. Previous discussions involve a stronger Arctic Dipole [*Overland and Wang*, 2010; *Blüthgen et al.*, 2012], enhanced blocking highs [*Liu et al.*, 2012; *Tang et al.*, 2013], and changes in jet stream characteristics and planetary wave propagation [*Jaiser et al.*, 2012; *Outten and Esau*, 2012; *Francis and Vavrus*, 2012]. While changes in horizontal planetary wave characteristics are debated [*Barnes*, 2013], there is strong evidence that vertical wave propagation and consequently the stratosphere play a major role in the Arctic to mid-latitude linkage [*Jaiser et al.*, 2013; *Manzini et al.*, 2014; *Kim et al.*, 2014; *Nakamura et al.*, 2015; *King et al.*, 2015, *Sun et al.*, 2015]. It is well known that planetary waves emanating from the troposphere propagate into the stratosphere and have the potential to weaken the polar vortex [*Matsuno*, 1971]. These anomalies then propagate downward from the upper stratosphere and reach the troposphere leading to negative Northern Annular Modes (NAMs) [*Baldwin and Dunkerton*, 1999, 2001; *Polvani and Waugh*, 2004]. In this way, negative NAM events can be related to reduced sea ice conditions as observations suggest for the recent decade. However, it has to be remarked that the manifestation of the tropospheric response is generally non-linear. It depends on the amount of sea ice loss [*Petoukhov and Semenov*, 2010] as well as on the location of sea ice loss [*Rinke et al.*, 2013; *Pedersen et al.*, 2015].

Snow cover changes have been also discussed as a driver of large scale atmospheric circulation changes emerging from the Arctic [*Cohen et al*., 2007]. *Cohen et al.* [2014] discussed Arctic sea ice and snow cover as cryospheric forcings that jointly influence mid-latitude weather.

The question arises whether both drivers are interrelated or independent with similar pathways and consequences. *Wegmann et al.* [2015] discussed a possible connection and found that the loss of sea ice could increase the autumn snow cover as ice free Arctic marginal seas are an increasing moisture source for the Eurasian continent. Nonetheless, the relative roles of sea ice and snow remain open in the question of Arctic to mid-latitude climate linkages.

Recently, *Nakamura et al.* [2015] showed that the Arctic sea ice reduction alone results in modulation of atmospheric circulation so as to weaken the polar vortex with a consequential negative shift of the phase of the NAM using a fully stratosphere resolving AGCM. Additional experiments with suppressed wave-mean flow interactions in the stratosphere have been performed by *Nakamura et al.* [2016] showing the crucial role of the stratosphere for these linkages. Extending their results, the present study aims to provide detailed information on vertical planetary wave propagation and thus the coupling between stratosphere and troposphere by means of the comparison between the model experiment of *Nakamura et al.* [2015] and the ERA-Interim reanalysis data with respect to low and high sea ice conditions in the Arctic. A particular focus is on timing and regional characteristics of both upward and downward propagation of signals.

2 Materials and Methods

This study implements a comparison between ERA-Interim reanalysis data and model simulations with respect to sea ice cover changes in the Arctic. ERA-Interim is the most recent available reanalysis performed by the ECMWF [*Dee and Uppala*, 2009]. The model has a spectral resolution of T255 with 60 model levels and a 0.1hPa model top with six hourly output. In this study we use daily data at 2° horizontal resolution from 1979 to 2014.

We selected two time periods to represent low and high sea ice conditions in ERA-Interim data. The selection of time periods for the analysis has to be balanced between short time periods for more pronounced sea ice differences and longer time periods for better statistics. In this study, we preferred long continuing time periods and will show that the actual sea ice anomalies are in very good agreement with anomalies based on shorter time periods. Furthermore, the selected periods are consistent with our previous studies [*Jaiser et al.* 2012, 2013], except for the addition of most recent winters. The period for high and low sea ice conditions are from 1979 until winter 1999/2000 and from 2000 until winter 2013/14, respectively. The results presented in this article are robust against small changes applied to the periods. We checked this by implementing the same periods as *Kug et al.* [2015] from 1979 until 1997 and from 1998 until 2013 for high and low ice conditions, respectively.

For the simulation results, we used the output of sensitivity experiments with respect to the Arctic sea ice reduction carried out by *Nakamura et al.* [2015]. They applied the atmospheric general circulation model for Earth Simulator (AFES) version 4.1 with a spectral resolution of T79, 56 vertical levels and a model top of about 60 km. They performed two perpetual model integrations labeled CNTL and NICE with 60 years each excluding spin up time, where only the prescribed sea ice conditions in the Arctic are different. High ice conditions in the CNTL experiment are obtained from the observed 1979 to 1983 average of sea ice concentration, whereas low ice conditions in the NICE experiment are obtained from the 2005 to 2009 period. The sea ice concentration data is linearly converted to sea ice thickness between 0 and 50 cm. This approach has been chosen to simulate the actual turbulent heat flux from the ocean to the atmosphere reasonably well as described in *Nakamura et al.* [2015]. Sea surface temperature

(SST) data is kept constant to its 1979 to 1983 mean value in both model runs. In the NICE experiment additional ice free regions appear. These regions have been filled with SST values from the early period as well. This allows for a consistent SST dataset without transitions between high and low ice condition SST and thus arbitrary SST gradients affecting the atmosphere. The compromise is a too low SST in newly ice free regions, leading to an underestimated forcing of the atmosphere from the ocean. In section 3.1 we compare the actual sea ice distribution for AFES and ERA-Interim.

By means of the experimental design of the AFES simulations, the sea ice implements seasonal variability but no year-to-year variability. Only sea ice differences between the CNTL and NICE model runs and internally generated variability induce anomalies in the atmospheric conditions. The experiment has two long time series with internally generated atmospheric variability, but it is not possible to calculate regressions or define composites due to the perpetual sea ice concentration in each run. In contrast, ERA-Interim exhibits year-to-year variability not only in sea ice but also in all other driving conditions as observed in recent years. Therefore, atmospheric signals are more diffused by processes that are not necessarily related to Arctic sea ice changes. This effect becomes relevant due to the relatively short time series of high quality reanalysis data from 1979 up to the present day. We validated if this affects our approach to use two long time periods instead of regressions or composites. In fact, the bias between low and high ice conditions of climate indices other than the expected AO response (*Nakamura et al.* 2015) becomes larger for composites than for our periods. Long periods tend to even out the effects of other climate forcing, while in composites one or more forcing factors tend to stand out for at least one of the samples. It is not possible to remove these from the composites, since then only individual years remain leading to a completely arbitrary analysis. Thus, the potential impact of unwanted forcing from outside the Arctic is larger for composites than for our periods. Most importantly and as mentioned before, the AFES experiment is designed more period-like and does not allow defining composites or regressions. Therefore we achieve the best comparability, if we keep as much internal variability as possible and use periods for the reanalysis.

In our analysis we will discuss figures showing the temporal evolution of anomalies. The corresponding data has been smoothed by calculating 21-day running mean values. This width for an averaging kernel was chosen for a balance between removing noise and keeping week-to-week variability. Besides climatological data from reanalysis and model simulations, we compute localized Eliassen Palm (EP) fluxes as defined by *Trenberth* [1986]. The EP flux vector points into the direction of wave propagation. We use the vertical component to diagnose vertical wave propagation. Flux data is filtered with a 2.5 to 6.5 days digital band-pass filter and a 10 to 90 days digital low-pass filter according to *Blackmon and Lau* [1980]. They provide anomalies associated with synoptic-scale motions (i.e. large scale high frequent eddies) and planetary-scale disturbances (i.e. planetary waves), respectively.

To characterize the strength of planetary waves in a horizontal plane we have calculated the amplitudes of waves with zonal wavenumbers one and two (ZWN1 and ZWN2) derived from the northern hemisphere geopotential height fields at each level and each time. To do this we have reconstructed the ZWN1 and ZWN2 fields from the full geopotential height fields by applying spherical harmonic analysis and spherical harmonic synthesis with truncation at total wave numbers 1 and 2 at each level and each time. The corresponding amplitudes of the planetary waves ZWN1 and ZWN2 have been calculated from the reconstructed ZWN1 and

ZWN2 fields, respectively. For performing spherical harmonic analysis and synthesis subroutines from the software package SPHEREPACK 3.2 has been used [Adams and Swarztrauber, 1999].

In the present study different levels of significance are shown at 90% (dotted), 95% (dashed) and 99% (solid) as denoted in the figures. The statistical test is based on a Mann-Whitney-Wilcoxon nonparametric rank-sum test (U test).

3 Results

3.1 Low and high sea ice conditions

Figure 1 shows a compilation of autumn and winter season mean Arctic sea ice concentration anomalies for the AFES model and the ERA-Interim reanalysis. Anomaly patterns show the difference NICE minus CNTL for AFES (Figure 1a and c) and low ice period minus high ice period for ERA-Interim (Figure 1b and d), respectively. Differences appear in the magnitude of anomalies, while their spatial distribution is in near perfect agreement. The differences in magnitude are explained by the averaging over more seasons in the ERA-Interim periods (21 high ice and 14 low ice seasons, respectively) and thus higher variability compared to the average over only 5 different seasons for each run in the AFES experiment. From the fact that the effect of smoothing is stronger in the ERA-Interim anomalies, we can expect a stronger atmospheric response in the AFES experiment not only due to the experimental setup with perpetual runs, but also due to the larger differences in averaged high and low sea ice conditions.

In autumn (Figure 1a and b), negative sea ice concentration anomalies cover all Arctic marginal seas with maximums around the East Siberian and Chukchi Seas as well as the Barents and Kara Seas. In AFES an additional positive anomaly exists in the Greenland Sea, where the sea ice extends farther east into the Fram Strait region. Towards winter (Figure 1c and d) the marginal seas freeze up rapidly, despite the previously large negative anomalies. The largest negative anomaly appears in the Barents Sea. Further notable areas for negative anomalies are in the Sea of Okhotsk and in the southern part of the Greenland Sea. The latter region shows a kind of a dipole pattern, where the western part close to the east coast of Greenland has a positive anomaly suggesting a more concentrated sea ice cover in low ice years with less frequent extensions far into the Greenland Sea where the negative anomaly is located. Another positive anomaly is located in the Bering Straight, but only in the AFES sea ice concentration. Overall, the regional characteristics of seasonal sea ice anomalies are very consistent between AFES and ERA-Interim, which warrants a coherent comparison of both data sets.

3.2 Atmospheric circulation impact in winter

In winter, planetary waves are allowed to propagate from the troposphere into the stratosphere due to the prevalence of westerly winds in these layers. The corresponding vertical component of planetary scale EP flux is shown in Figure 2 as the difference between low and high sea ice conditions. This illustrates the change in the vertical propagation of planetary waves. The polar cap average (65°N-85°N and 0°E-360°E) of vertical EP flux difference NICE minus CNTL in the AFES experiment (Figure 2a) is positive starting in November and continues throughout December, at which the positive signal enters the stratosphere. Similar anomalies are present in ERA-Interim (Figure 2b), but show less significance and are more disturbed by short periods of negative vertical EP flux differences. Upward propagating planetary waves are

generated in the troposphere underpinning the relationship to sea ice changes. Later they reach the stratosphere and interact with the polar vortex.

In the difference between the NICE and CNTL run (Figure 2a) strong negative planetary-scale EP flux anomalies start in mid-January. The signal is significant in the troposphere, while it is more disturbed in the stratosphere. This continues into February, when a significant negative anomaly becomes visible from the lower stratosphere down to the troposphere. The negative anomaly is related to an interruption of upward propagating planetary waves for low ice conditions. While in the CNTL run planetary waves still propagate into the stratosphere in February, this is not the case in the NICE run (not shown here). The absence of vertical wave propagation is an indication of a stratospheric polar vortex breakdown. In the ERA-Interim data (Figure 2b) the negative anomaly clearly starts in the beginning of February without preceding negative anomalies in the troposphere or stratosphere. Again the vertical propagation of planetary waves into the stratosphere is reduced under low sea ice conditions with weak indications of actual downward EP flux (not shown here).

To support our hypothesis on the timing of the vertical propagation of planetary waves, first intensified in early winter and then reduced in February following reduced sea ice conditions, we performed a wave amplitude analysis. Figure 3 shows differences between low and high sea ice conditions of the average maximum amplitudes of ZWN1 (Figure 3a and c) and ZWN2 (Figure 3b and d) as height over time cross-section for the Arctic region in AFES (Figure 3a and b) and ERA-Interim (Figure 3c and d). In late autumn and early winter overall positive anomalies are found in both data sets. Enhanced ZWN1 anomalies beginning in October show generally higher magnitudes in ERA-Interim. A period of lower ZWN1 amplitudes occurs in late November and early December, which is consistent between AFES and ERA-Interim. The preceding positive anomalies manifest as periodical pulses from the troposphere into the stratosphere. Later in December a strong positive ZWN1 anomaly is visible in the higher stratosphere that propagates downward with time. In accordance with a vortex breakdown induced by large scale planetary waves the anomaly switches to negative in late January and February in the stratosphere. This event is observed about one or two weeks earlier in ERA-Interim. Generally, the amplitude differences diagnosed for ZWN1 are smaller in AFES and in particular the positive anomalies are restricted to the upper stratosphere. Additional positive anomalies throughout the whole troposphere and stratosphere are found for ZWN2 from November to January in AFES. In February the anomalies switch to negative sign consistent with ZWN1. ZWN2 in ERA-Interim shows a strong pulse of enhanced amplitudes in early December throughout the whole troposphere and stratosphere. This pulse precedes the positive ZWN1 anomaly indicating conversion from ZWN2 to ZWN1 in the upper stratosphere. A second positive ZWN2 anomaly is observed in early January simultaneous to the positive ZWN1 anomaly. Generally, the wave amplitude analysis is in agreement with our findings on the vertical propagation of planetary waves.

It should be mentioned, that the analysis based on the vertical component of EP flux and the wave amplitude analysis of geopotential heights do not necessarily describe the same physical phenomena. While the EP flux diagnostics is designed to show changes in the vertical propagation of planetary waves, the wave amplitude analysis diagnoses changes of the intensity of horizontal waves. In the reduced sea ice case discussed here, the agreement between vertical wave propagation and horizontal wave amplitudes is good. This supports our hypothesis of large scale planetary waves with ZWN1 and ZWN2 propagating into the stratosphere in early winter

leading to a vortex breakdown around the beginning of February. When the vortex breaks down, vertical propagation of planetary waves is reduced along with reduced horizontal wave amplitudes. The design of the AFES experiment and the agreement with the selected ERA-Interim time periods clearly suggest that sea ice anomalies are a driver for those observations.

A breakdown of the stratospheric polar vortex leads to anomalies in the atmospheric circulation apart from planetary wave propagation. Figure 4 shows zonal wind, geopotential heights, temperature and synoptic-scale heat flux averaged over the polar cap (65°N-85°N and 0°E-360°E) and difference between low and high sea ice conditions. The most prominent feature in the vertical component of EP flux (Figure 2) was the change from positive to negative anomalies around the beginning of February. Consistently zonal wind (Figure 4a and b), geopotential heights (Figure 4c and d) and temperature (Figure 4e and f) all show coherent anomalies. The zonal wind is reduced to zero or negative (easterly) for lower sea ice conditions in both AFES (Figure 4a) and ERA-Interim (Figure 4b) data.

In early winter, zonal winds were slightly enhanced for low sea ice conditions. This might be related to an enhanced wave driven polar vortex before it becomes unstable from overly intensive wave disturbances. Corresponding slightly negative wind anomalies are first seen in January and thus in coincidence with the strongest upward propagating planetary wave anomaly. Then in February the vortex breaks down. Along with the negative stratospheric wind anomalies due to the vortex breakdown a strong positive geopotential height anomaly appears throughout troposphere and stratosphere in late January (Figure 4c and d). This is consistent with a negative Northern Annular Mode (NAM) related to the vortex breakdown. A first pulse of enhanced geopotential heights is visible in December and is related to the upward planetary wave propagation. Generally the positive geopotential heights are related to a positive temperature signal (Figure 4e and f). In the stratosphere this warming and higher pressure signal are consistent with a downdraft of the atmosphere induced by the vortex breakdown. In the troposphere more meandering waves induce an intensified meridional mixing. This and the suggested winter negative NAM phase in the troposphere are further supported by negative anomalies in the synoptic scale heat fluxes (Figure 4g and h). Reduced synoptic scale eddies contribute to blocking situations as discussed by other studies [e.g., *Francis and Vavrus*, 2012; *Liu et al.*, 2012] consistent with a negative NAM phase.

The process leading to a vortex breakdown is explained by intensified upward propagating planetary waves that disturb the vortex and thus consistent with other studies [Baldwin and Dunkerton, 2001; Polvani and Waugh, 2004]. Due to the vortex breakdown, the stratospheric westerlies disappear and planetary wave propagation into the stratosphere is prohibited [Charney and Drazin, 1961]. This leads to the negative vertical planetary scale EP flux anomalies in February as seen in Figure 2. These negative anomalies extend into the troposphere and are also visible in the horizontal wave amplitudes for ZWN1 and ZWN2. The stratospheric signal reaches the troposphere through the changed vertical wave structure and through changed geopotential heights following to the vortex breakdown in the stratosphere.

The largest differences between AFES (left column in Figure 4) and ERA-Interim (right column in Figure 4) appear in the fields of geopotential heights (Figure 4c and d) and temperature (Figure 4e and f) throughout the year. In ERA-Interim, a warmer troposphere and colder stratosphere are diagnosed along with generally higher geopotential heights. This is largely related to a global warming signal induced by increasing CO2 and related forcing factors. In AFES, every forcing is kept constant except for sea ice anomalies, thus this effect is absent

there. Therefore, only a near-surface warming is visible in autumn. One additional consistent anomaly between AFES and ERA-Interim appears in late October and early November. Figure 4 shows a positive wind anomaly in the troposphere also reaching the stratosphere in coincidence with enhanced synoptic scale heat fluxes in the lower and middle troposphere. This indicates a wind forcing induced by synoptic scales anomalies that reach the stratosphere contributing to some kind of preconditioning. Especially in AFES the wind anomaly is significant in October and November and weakly connects to the stratosphere where the positive wind anomaly persists until the vortex breakdown occurs as discussed above. This suggests a relation of the winter vortex breakdown to autumn synoptic scale changes. Noticeable is that these autumn anomalies appear later in ERA-Interim than in AFES.

There is a high degree of consistency between ERA-Interim and AFES data especially in the crucial winter timeframe. Most anomalies associated with the changes between low and high sea ice conditions are present in both data sets. The level of significance varies but is mostly higher in the simulations, in which no apparent competing processes exist because of the experimental setup. Also the timing of anomalies is highly consistent between both data sets and varies only in the order of one or two weeks.

The discussion here is based on averaged multi-year time periods to achieve an optimal comparability between the model experiment with perpetual years and the reanalysis as well as to perform a statistically reliable analysis. With this approach variability exists in both datasets. It is generated from non-linear variability in AFES and ERA-Interim and additional external forcing in ERA-Interim only. Stratospheric year-to-year variance of wind, temperature and geopotential heights is about 10% larger averaged over the polar cap in ERA-Interim due to the additional forcing. Under low ice conditions, an increase of year-to-year variability appears in early winter in both datasets in agreement with more frequent vortex breakdowns in this time frame. A closer inspection of all single years indicates that a vortex breakdown or a vortex weakening does not occur in every low ice year in January or February. The atmosphere is more vulnerable to early vortex breakdowns, but is still affected by natural variability that may be inhibiting vortex breakdowns or shifting them within the season. Especially stratospheric internal variability is large and may inhibit an external signal to impact the circulation [*Scott and Polvani* 2006; *Scott et al.* 2008]. Related decadal variability in ERA-Interim will be discussed separately in section 3.4.

3.3 Regional aspects of vertical planetary wave propagation

The polar cap averaged quantities do not describe which Arctic regions control the vertical planetary wave propagation anomalies. Figure 5 shows the vertical component of the planetary scale EP flux component at 300 hPa in December. This level is close to the Arctic tropopause and thus characterizes waves that actually reach the stratosphere. Northward of 60°N two regions stand out: The Barents and Kara Sea region (BKS region) and the Arctic sector towards the Pacific (Pacific region). Additional anomalies are found over the eastern part of Canada and over the Atlantic. The main center of action of the latter anomalies lies more in the mid-latitudes, exposing it to other external forcing than sea ice. This is assured by the stronger anomaly in the ERA-Interim data (Figure 5b), while the anomaly is weaker in the AFES experiment (Figure 5a), suggesting that the anomaly is not primarily sea ice related. Furthermore, an analysis of the height dependent temporal behavior of the vertical component of the EP flux in this region shows no notable anomalies that connect troposphere and stratosphere through

upward propagating planetary wave anomalies despite the anomalies at the tropopause in December. Actually, the strongest stratospheric upward EP flux anomaly in this region occurs just after the vortex breakdown and is therefore not part of the discussion here.

The anomalies in the BKS region and the Pacific region form two hotspots for upward planetary wave propagation in the Arctic. They are consistently found in AFES (Figure 5a) and ERA-Interim (Figure 5b). Significance levels are higher for the AFES simulations, which is again attributed to the more disturbed nature of the ERA-Interim results arising from other forcings. This further suggests a strong relation to sea ice anomalies. Based on the analysis of the full three-dimensional data, the area from 65°N to 85°N and from 30°E to 90°E has been defined as the BKS region, while the and the Pacific region has been defined to cover 65°N to 85°N and 150°E to 120°W. The corresponding time and height dependent analysis of the vertical component of planetary scale EP flux is shown in Figure 6.

In Figure 2 the vortex breakdown was diagnosed starting in February after a period of intensified upward planetary wave propagation under low sea ice conditions. Figure 6 shows that the upward propagation anomaly does not occur simultaneously in the two different regions. For the AFES experiment the upward signal is seen in mid-November throughout the troposphere and stratosphere over the BKS region (Figure 6a). It appears after a period with extensive upward EP flux in the troposphere starting just before October. Since the sea ice anomaly is largest in the BKS seas this suggests a direct sea ice influence. At this time in October the upward planetary wave propagation cannot reach the stratosphere, because the required stratospheric westerly wind is still in the process of building up. Then in mid-November upward wave propagation into the stratosphere begins. The November anomaly in the BKS region is consistently represented in ERA-Interim (Figure 6b), although the tropospheric part does not start until November. Generally the signal is more disturbed, less intense and less significant than in the AFES simulations.

Following to this event we find a second pulse of upward planetary wave propagation over the Pacific region (Figure 6c and d) starting in the mid-December just until the vortex breakdown in late January or February with a strong negative anomaly in the vertical component of EP flux on planetary scales. It is again preceded by a period of intensified tropospheric upward propagation starting in November suggesting a tropospheric source. This anomaly is also consistent between AFES (Figure 6c) and ERA-Interim (Figure 6d). One major difference between model and reanalysis data is the earlier appearance of the switch to a negative anomaly seen in ERA-Interim. This is consistent with the discussion of Figure 3 and Figure 4, where clear signals of an earlier vortex breakdown in ERA-Interim were found for horizontal wave amplitudes and climatological quantities, respectively.

The consistency of the switch from a positive vertical EP flux anomaly to a negative between the Pacific region (Figure 6c and d) and the full polar cap anomalies (Figure 2) further suggests that the Pacific upward anomaly is the primary trigger of the vortex breakdown. The negative anomaly in February is more clearly diagnosed in the Pacific region than in the BKS region. To some extent this is explained by the general winter upward planetary wave propagation which is stronger over the Pacific region (not shown). The common characteristics of the negative anomaly are a recess of upward wave propagation due to the vortex breakdown with only weak actual downward wave propagation. Therefore a strong negative anomaly showing the disruption of climatological upward wave propagation can only be expected over the Pacific region, where the climatological pattern shows the strongest upward propagation.

We have found two regions of major anomalies for upward planetary wave propagation on opposing sites of the Arctic in the BKS region and on the Pacific side of the Arctic. In a conceptual framework they form a wave number 2 anomaly that is sufficient to deform the polar vortex leading to the observed stratospheric polar vortex breakdown in February. Both anomalies do not appear simultaneously, thus the BKS anomaly acts as a preconditioning. The study of *Sun et al.* [2015] shows, if sea ice is reduced in the Atlantic sector, vertical wave propagation exhibits similar anomalies like in the present study. In contrast, if sea ice is reduced in the Pacific region, vertical wave propagation shows a different inverse response. In agreement with the small sea ice reduction in the Pacific region in winter in our experiment, we conclude that sea ice in the BKS region is the source of vertical wave propagation anomalies. Thus, it is reasonable that the BKS anomaly occurs first, indicating the direct sea ice induced forcing. The link to the Pacific region upward planetary wave propagation anomaly might be established through horizontal wave propagation as discussed in *Honda et al.* [2009]. They showed that sea ice anomalies in the BKS region impact the horizontal planetary wave over Siberian continental areas. This has the potential to change the climatological wave propagation in the Pacific region to the observed enhanced upward propagation, while the detailed mechanism needs further research. For the corresponding AFES experiments, *Nakamura et al.* [2015, 2016] show that the BKS region indeed intensifies the climatological planetary-scale wave along the Asian continent, which is preferable to disturb the stratospheric polar vortex.

3.4 Decadal variability

Processes in the stratosphere play a key role in explaining the impact of sea ice changes on the large-scale atmospheric circulation. Variability in the stratosphere itself is rather strong on decadal time scales. This can be seen if the reference period with high sea ice conditions is split into two periods. We chose the 80s (1979/1980 to 1989/1990) and the 90s (1990/1991 to 1999/2000) decades. *Hitchcock et al.* [2013] showed 8 sudden stratospheric warmings (SSWs) occurring in the 80s decade compared to only 2 in the 90s decade. Their data further indicates 9 SSWs between 2000/2001 and 2009/2010 covering almost the entire low ice period, which is a similar rate of SSWs as in the 80s decade. For cross-validation we use the FU Berlin data set based on *Muench and Borden* [1962] and *Labitzke and Naujokat* [2000]. They determined major mid-winter warmings and major final warmings that are in good agreement with *Hitchcock et al.* [2013]. There were 9 warmings in the 80s decade, 1 in the 90s decade and 11 between 2000/2001 and 2012/2013. A hypothesis to test is whether a less stable polar vortex in the low ice period is a residual anomaly due to the low SSW count in the 90s decade. In this study we validate this by comparing the low ice period in ERA-Interim to the reference decades 80s and 90s separately.

The upward planetary scale EP flux anomaly in early winter is disturbed regardless of the reference period. The strongest signal is found in the AFES experiment (Figure 2a) while ERA-Interim (low minus high in Figure 2b, low minus 80s decade in Figure 7a and low minus 90s decade in Figure 7b) barely shows significant indications of strong upward EP flux anomalies for the polar cap average. Nevertheless, the downward part in February is clearly visible, especially if the 80s decade is the reference period. This is rather unexpected, since the 80s decade showed a high SSW count more similar to the low ice period. Larger downward anomalies would have been expected if the low ice period is compared to the 90s decade with only few SSWs and thus a stronger and more stable stratospheric polar vortex. This is a clear sign of a sea ice induced process that is different from the decadal variability between the 80s and 90s decades.

Geopotential height and zonal wind data are analyzed in the same separated periods in addition to the vertical planetary wave propagation as shown in Figure 7. The positive GPH anomaly is strongest if low sea ice conditions are compared to the 90s decade (Figure 7d). This result is less unexpected, as the positive NAM phase in the 90s decade leads to stronger and more significant differences if compared to the more negative NAM phase under low sea ice conditions. But the positive geopotential heights anomaly is also visible if only the 80s decade is taken into account. The generally higher geopotential heights under low sea ice conditions in all seasons are independent from decadal variability and thus are also in agreement with global climate change and the generally warmer Arctic.

Zonal wind anomalies are different depending on height. On the one hand, if low sea ice conditions are compared to the 80s decade (Figure 7e), a significant negative anomaly exists most notably in the troposphere in February. On the other hand, if low sea ice conditions are compared to the 90s decade (Figure 7f), significant negative wind anomalies dominate the stratosphere in February. The latter fact is easily explained by missing SSWs in the 90s decade and therefore a persistent polar vortex in late winter and early spring. But this does not impact the troposphere, indicating that tropospheric westerlies were relatively weak in the Arctic in the 90s decade despite the positive NAM and the strong polar vortex. If low sea ice conditions are compared to the 80s decade, the stratospheric wind anomalies are negative in winter, but only slightly significant at the end of February. SSWs exist in the 80s decade as well as in the sea low ice period. Therefore a large variability of vortex strength is observed in both periods leading to almost no significant differences. Still, the short significant negative anomaly and the generally lower zonal winds indicate that weak vortex events are more dominant in the low ice period. Furthermore the significant part at the end of February clearly connects to the troposphere. This shows the unique control of stratospheric winds on the troposphere in the low ice period which could be related to the extraordinary strength of negative wind anomalies.

Generally the planetary wave forcing and climatological differences are consistent with our sea ice hypothesis. Large anomalies in the fields of the vertical component of planetary scale EP flux, geopotential heights and wind are always observed for low sea ice conditions regardless of the reference period, but with varying significance. It is unexpected that the largest negative anomaly of vertical planetary wave propagation is observed if the period of low sea ice conditions is compared to the 90s decade, but this confirms the influence of sea ice in two ways: First, the sea ice extent and volume difference is largest if the 80s decade is taken as a reference. Second, the stratospheric variability is more comparable between 80s decade and the low ice period in terms of SSWs. Therefore the stratospheric internal variability is less likely the underlying cause of the observed large differences in the troposphere and stratosphere described in this study underpinning the impact of sea ice changes.

4 Conclusions

The design of the model experiment discussed here allows for a dedicated analysis of the impact of sea ice extent anomalies on the atmosphere. Since every other forcing and boundary condition is kept constant in the model runs, we can deduce differences in atmospheric processes forced by the prescribed sea ice changes. The outstanding agreement in Arctic regions between the model experiment and reanalysis in terms of vertical planetary wave propagation in the troposphere and stratosphere provides strong evidence that atmospheric circulation changes induced by sea ice changes are one of the dominant winter climate impacts in recent years. Only

weak differences are present between model and reanalysis data, therefore other processes contribute less to similar anomalies that only slightly modify the sea ice signal.

Nevertheless, other processes are important, indicated by the comparison between model and reanalysis outside the winter timeframe. Since the change in greenhouse gas concentrations is not implemented in the model experiment, Arctic warming is missing in seasons outside the northern winter. To analyze the full impact of global climate change experiments driven by a full set of boundary conditions are needed. These are prepared for the AFES model. Previous studies with ECHAM6 runs show that these more complex simulations do not necessarily lead to clear results [*Handorf et al.*, 2015]. Here we argue two potential sources of differences between the studies based on ECHAM6 and AFES runs. First, the overall implementation of sea ice is more thoughtfully done in the AFES model experiment. With the conversion of observed sea ice concentrations to sea ice thickness with a maximum of 0.5m a much better representation of turbulent heat fluxes from the ocean to the atmosphere through the sea ice has been achieved. Second, the model driven by a complete set of varying boundary conditions has to deal with more complex interactions of processes in the atmosphere and is therefore far more sensible to any disturbances. Such an experiment is therefore more susceptible to show a different climate regime due to only small deviations in climate forcings. The only way to overcome these issues is to have more model studies of both kinds with different models.

One Arctic impact factor that has always been discussed in relation to sea ice is snow. Observational studies show very similar impacts of snow and sea ice changes on the winter atmosphere [*Vihma*, 2014; *Cohen et al.*, 2014]. In fact the model experiment exploited here does not show snow variance in accordance with the observed anomalies. Therefore the discussion of snow impacts is limited, but there are two first order conclusions. First it indicates that snow and sea ice impacts are well separated. Although this could still allow for interactions between both cryospheric forcings and they may modify each other. Second, the early winter differences between the model experiment and the reanalysis as well as timing differences may be explained by the missing snow impacts in the model experiment. The atmospheric circulation and planetary wave propagation differences between low and high ice conditions are generally stronger in ERA-Interim, which could be explained by additional snow related forcing.

The overall good agreement between model experiment and reanalysis allows for more detailed analysis of regional aspects. We identified two regions that play a particular role for vertically propagating planetary waves. One is the Barents and Kara Sea region and the other one is located around the Beaufort, Chukchi and East Siberian Sea. These two regions are also the ones with the largest observed sea ice anomalies and thus with large sea ice impact being expected. This is especially true for the BKS region, since here the sea ice anomaly persists in winter. The opposite position of the anomalies of upward propagating planetary waves further implies a wave number 2 forcing, although the anomalies occur not simultaneously. Accordingly, we diagnose a mixed wave number 1 and 2 response leading to displacement and deformation of the stratospheric polar vortex and finally a breakdown around the beginning of February. The BKS anomaly occurs in late November and December and acts as some kind of preconditioning. The Pacific region anomaly appears late December and January and thus just before the vortex breakdown.

The timing of various anomalies is very consistent between the AFES model and the ERA-Interim reanalysis differing only within weeks. Also on longer time scales we find consistent results. Stratospheric variability in terms of SSWs does not influence our conclusions

on the impact of sea ice anomalies on the atmospheric large-scale circulation. This robustness provides some degree of potential predictability for mid-latitudes by Arctic regions as suggested by *Jung et al.* [2014].

Acknowledgments and Data

The ERA interim data were obtained from the ECMWF web site (http://data-portal.ecmwf.int/). The AFES simulations were performed on the Earth Simulator at the Japan Agency for Marine–Earth Science and Technology (JAMSTEC). Merged Hadley–NOAA/OI SST and SIC data were obtained from the Climate Data Guide provided by the National Center for Atmospheric Research (NCAR) and University Corporation for Atmospheric Research (UCAR) (https://climatedataguide.ucar.edu/). Freie Universität Berlin analyses (FUB-analysis) data set on North Pole temperatures is openly available from their website (http://www.geo.fu-berlin.de/en/met/ag/strat/produkte/northpole/index.html). SPHEREPACK 3.2 is distributed under the SPHEREPACK Software License (https://www2.cisl.ucar.edu/resources/legacy/spherepack). RJ, DH and KD acknowledge the support of the HGF REKLIM project. TN, KY and JU acknowledge the support of the Green Network of Excellence Program (GRENE Program) Arctic Climate Change Research Project and the Arctic Challenge for Sustainability (ArCS) project. We thank three anonymous reviewers for their constructive comments.

References

Adams, J. C., and P. N. Swarztrauber (1999), SPHEREPACK 3.0: A model development facility, Monthly Weather Review, 127(8), 1872-1878, doi:10.1175/1520-0493(1999)127<1872:SAMDF>2.0.CO;2.

Alexeev, V. A., I. Esau, I. V. Polyakov, S. J. Byam, and S. Sorokina (2012), Vertical structure of recent Arctic warming from observed data and reanalysis products, Climatic Change, 111(2), 215-239, doi:10.1007/s10584-011-0192-8.

Baldwin, M. P., and T. J. Dunkerton (1999), Propagation of the Arctic Oscillation from the stratosphere to the troposphere, Journal of Geophysical Research: Atmospheres (1984–2012), 104(D24), 30937-30946, doi:10.1029/1999JD900445.

Baldwin, M. P., and T. J. Dunkerton (2001), Stratospheric harbingers of anomalous weather regimes, Science, 294(5542), 581-584, doi:10.1126/science.1063315.

Barnes, E. A. (2013), Revisiting the evidence linking Arctic amplification to extreme weather in midlatitudes, Geophysical Research Letters, 40(17), 4734-4739, doi:10.1002/grl.50880.

Blackmon, M. L., and N. C. Lau (1980), Regional characteristics of the Northern Hemisphere wintertime circulation: A comparison of the simulation of a GFDL general circulation model with observations, Journal of the Atmospheric Sciences, 37(3), 497-514, doi:10.1175/1520-0469(1980)037<0497:RCOTNH>2.0.CO;2.

Blüthgen, J., R. Gerdes, and M. Werner (2012), Atmospheric response to the extreme Arctic sea ice conditions in 2007, Geophysical Research Letters, 39(2), doi:10.1029/2011GL050486.

Charney, J. G., and P. G. Drazin (1961), Propagation of planetary scale disturbances from the lower into the upper atmosphere, Journal of Geophysical Research, 66(1), pp. 83–109, doi:10.1029/JZ066i001p00083.

Cohen, J., M. Barlow, P. J. Kushner, and K. Saito (2007), Stratosphere-troposphere coupling and links with Eurasian land surface variability, Journal of Climate, 20(21), 5335-5343, doi:10.1175/2007JCLI1725.1.

Cohen, J., J. A. Screen, J. C. Furtado, M. Barlow, D. Whittleston, D. Coumou, J. Francis, K. Dethloff, D. Entekhabi, J. Overland, and J. Jones (2014), Recent Arctic amplification and extreme mid-latitude weather, Nature geoscience, 7(9), 627-637, doi:10.1038/ngeo2234.

Dee, D. P., and S. Uppala (2009), Variational bias correction of satellite radiance data in the ERA-Interim reanalysis, Quarterly Journal of the Royal Meteorological Society, 135(644), 1830-1841, doi:10.1002/qj.493.

Francis, J. A., and S. J. Vavrus (2012), Evidence linking Arctic amplification to extreme weather in mid-latitudes, Geophysical Research Letters, 39(6), doi:10.1029/2012GL051000.

Handorf, D., R. Jaiser, K. Dethloff, A. Rinke, and J. Cohen (2015), Impacts of Arctic sea ice and continental snow cover changes on atmospheric winter teleconnections, Geophysical Research Letters, 42(7), 2367-2377, doi:10.1002/2015GL063203.

Hitchcock, P., T. G. Shepherd, and G. L. Manney (2013), Statistical characterization of Arctic polar-night jet oscillation events, Journal of Climate, 26(6), 2096-2116, doi:10.1175/JCLI-D-12-00202.1.

Honda, M., Inoue, J., and Yamane, S. (2009), Influence of low Arctic sea-ice minima on anomalously cold Eurasian winters, Geophysical Research Letters, 36(8), doi:10.1029/2008GL037079.

Jaiser, R., K. Dethloff, D. Handorf, A. Rinke, and J. Cohen (2012), Impact of sea ice cover changes on the Northern Hemisphere atmospheric winter circulation, Tellus A, 64, doi:10.3402/tellusa.v64i0.11595.

Jaiser, R., K. Dethloff, and D. Handorf (2013), Stratospheric response to Arctic sea ice retreat and associated planetary wave propagation changes, Tellus A, 65, doi: 10.3402/tellusa.v65i0.19375.

Jung, T., M. A. Kasper, T. Semmler, and S. Serrar (2014), Arctic influence on subseasonal midlatitude prediction, Geophysical Research Letters, 41(10), 3676-3680, doi:10.1002/2014GL059961.

Kim, B. M., Son, S. W., Min, S. K., Jeong, J. H., Kim, S. J., Zhang, X., Shim, T., and Yoon, J. H. (2014), Weakening of the stratospheric polar vortex by Arctic sea-ice loss, Nature communications, 5, doi:10.1038/ncomms5646.

King, M. P., M. Hell, and N. Keenlyside (2015), Investigation of the atmospheric mechanisms related to the autumn sea ice and winter circulation link in the Northern Hemisphere, Climate Dynamics, 1-11, doi:10.1007/s00382-015-2639-5.

Kug, J. S., J. H. Jeong, Y. S. Jang, B. M. Kim, C. K. Folland, S. K. Min, and S. W. Son (2015), Two distinct influences of Arctic warming on cold winters over North America and East Asia. Nature Geoscience 8, 759–762, doi:10.1038/ngeo2517

Labitzke, K. and B. Naujokat (2000), The lower arctic stratosphere in winter since 1952, SPARC Newsletter No.15, 11-14.

Liu, J., J. A. Curry, H. Wang, M. Song, and R. M. Horton (2012), Impact of declining Arctic sea ice on winter snowfall, Proceedings of the National Academy of Sciences, 109(11), 4074-4079, doi:10.1073/pnas.1114910109.

Manzini, E., A. Y. Karpechko, J. Anstey, M. P. Baldwin, R. X. Black, C. Cagnazzo, N. Calvo, A. Charlton-Perez, B. Christiansen, P. Davini, E. Gerber, M. Giorgetta, L. Gray, S. C. Hardiman, Y.-Y. Lee, D. R. Marsh, B. A. McDaniel, A. Purich, A. A. Scaife, D. Shindell, S.-W. Son, S. Watanabe, and G. Zappa (2014), Northern winter climate change: Assessment of uncertainty in CMIP5 projections related to stratosphere-troposphere coupling, Journal of Geophysical Research: Atmospheres, 119(13), 7979-7998, doi:10.1002/2013JD021403.

Matsuno, T. (1971), A dynamical model of the stratospheric sudden warming, Journal of the Atmospheric Sciences, 28(8), 1479-1494, doi:10.1175/1520-0469(1971)028<1479:ADMOTS>2.0.CO;2.

Muench, H. S., and T. R. Borden (1962), Atlas of monthly mean stratosphere charts, 1955-1959: Part I, January-June; Part II, July-December, Air Force Surveys in Geophysics No. 141.

Nakamura, T., K. Yamazaki, K. Iwamoto, M. Honda, Y. Miyoshi, Y. Ogawa, and J. Ukita (2015), A negative phase shift of the winter AO/NAO due to the recent Arctic sea-ice reduction in late autumn, Journal of Geophysical Research: Atmospheres, 120(8), 3209-3227, doi:10.1002/2014JD022848.

Nakamura, T., K. Yamazaki, K. Iwamoto, M. Honda, Y. Miyoshi, Y. Ogawa, Y. Tomikawa, and J. Ukita (2016), The stratospheric pathway for Arctic impacts on midlatitude climate, Geophys. Res. Lett., 43, doi:10.1002/2016GL068330.

Outten, S. D., and I. Esau (2012), A link between Arctic sea ice and recent cooling trends over Eurasia, Climatic Change, 110(3-4), 1069-1075, doi:10.1007/s10584-011-0334-z.

Overland, J. E., and M. Wang (2010), Large-scale atmospheric circulation changes are associated with the recent loss of Arctic sea ice, Tellus A, 62(1), 1-9, doi:10.1111/j.1600-0870.2009.00421.x.

Pedersen, R., I. Cvijanovic, P. Langen, and B. Vinther (2015), The impact of regional Arctic sea ice loss on atmospheric circulation and the NAO, J. Climate, doi:10.1175/JCLI-D-15-0315.1, in press.

Petoukhov, V., and V. A. Semenov (2010), A link between reduced Barents-Kara sea ice and cold winter extremes over northern continents, Journal of Geophysical Research: Atmospheres (1984–2012), 115(D21), doi:10.1029/2009JD013568.

Pithan, F., and T. Mauritsen (2014), Arctic amplification dominated by temperature feedbacks in contemporary climate models, Nature Geoscience, 7(3), 181-184, doi:10.1038/ngeo2071.

Polvani, L. M., and D. W. Waugh (2004), Upward wave activity flux as a precursor to extreme stratospheric events and subsequent anomalous surface weather regimes, Journal of climate, 17(18), 3548-3554, doi:10.1175/1520-0442(2004)017<3548:UWAFAA>2.0.CO;2.

Rinke, A., K. Dethloff, W. Dorn, D. Handorf, and J. C. Moore (2013), Simulated Arctic atmospheric feedbacks associated with late summer sea ice anomalies, Journal of Geophysical Research: Atmospheres, 118(14), 7698-7714, doi:10.1002/jgrd.50584.

Scott, R. K. and L. M. Polvani (2006), Internal Variability of the Winter Stratosphere. Part I: Time-Independent Forcing, Journal of the Atmospheric Sciences 63(11), 2758-2776, doi:10.1175/JAS3797.1

Scott, R. K., L. M. Polvani, and D. W. Waugh (2008), Internal Variability of the Winter Stratosphere. Part II: Time-Dependent Forcing, Journal of the Atmospheric Sciences 65(7), 2375-2388, doi:10.1175/2007JAS2619.1

Stroeve, J. C., M. C. Serreze, M. M. Holland, J. E. Kay, J. Malanik, and A. P. Barrett (2012), The Arctic's rapidly shrinking sea ice cover: a research synthesis, Climatic Change, 110(3-4), 1005-1027, doi:10.1007/s10584-011-0101-1.

Sun, L., C. Deser, and R. A. Tomas (2015), Mechanisms of Stratospheric and Tropospheric Circulation Response to Projected Arctic Sea Ice Loss, Journal of Climate, 28(19), 7824-7845, doi:10.1175/JCLI-D-15-0169.1

Tang, Q., X. Zhang, X. Yang, and J. A. Francis (2013), Cold winter extremes in northern continents linked to Arctic sea ice loss, Environmental research letters, 8(1), 014036, doi:10.1088/1748-9326/8/1/014036.

Taylor, P. C., M. Cai, A. Hu, J. Meehl, W. Washington, and G. J. Zhang (2013), A decomposition of feedback contributions to polar warming amplification, Journal of Climate, 26(18), 7023-7043, doi:10.1175/JCLI-D-12-00696.1.

Trenberth, K. E. (1986), An assessment of the impact of transient eddies on the zonal flow during a blocking episode using localized Eliassen-Palm flux diagnostics, Journal of the atmospheric sciences, 43(19), 2070-2087, doi:10.1175/1520-0469(1986)043<2070:AAOTIO>2.0.CO;2.

Vihma, T. (2014), Effects of Arctic sea ice decline on weather and climate: A review, Surveys in Geophysics, 35(5), 1175-1214, doi:10.1007/s10712-014-9284-0.

Wegmann, M., Y. Orsolini, M. Vázquez, L. Gimeno, R. Nieto, O. Bulygina, R. Jaiser, D. Handorf, A. Rinke, K. Dethloff, A. Sterin, and S. Brönnimann (2015), Arctic moisture source for Eurasian snow cover variations in autumn, Environmental Research Letters, 10(5), 054015, doi:10.1088/1748-9326/10/5/054015.

Figure Captions

Figure 1: Sea ice concentration anomalies (%) between low and high ice conditions for different seasons. (a, b) autumns season September to October, (c, d) winter season December to February; (a,c) AFES NICE minus CNTL, (b, d) ERA-Interim low ice period minus high ice period

Figure 2: Vertical component of planetary scale EP flux (m^2/s^2) averaged over 65°N-85°N and 0°E-360°E as 21 day running mean time vs. height plot. (a) AFES NICE minus CNTL, (b) ERA-Interim low ice minus high ice period. Significance on 90% (dotted), 95% (dashed) and 99% (solid) level marked in black contours.

Figure 3: Maximum wave amplitude analysis (gpm). (a, b) zonal wave number 1, (c, d) zonal wave number 2; (a, c) AFES NICE minus CNTL, (b, d) ERA-Interim low ice minus high ice period.

Figure 4: Climatological quantities averaged over 65°N-85°N and 0°E-360°E as 21 day running mean time vs. height plot. (a,b) zonal wind (m/s), (c,d) Geopotential heights (gpm), (e,f) temperature (K), (g,h) synoptic scale heat flux (Km/s) (a,c,e,g) AFES NICE minus CNTL, (b,d,f,h) ERA-Interim low ice minus high ice period; Significance on 90% (dotted), 95% (dashed) and 99% (solid) level marked in black contours.

Figure 5: Vertical component of planetary scale EP flux (m^2/s^2) in 300 hPa in December. (a) AFES NICE minus CNTL, (b) ERA-Interim low ice minus high ice period. Significance on 90% (dotted), 95% (dashed) and 99% (solid) level marked in black contours.

Figure 6: Vertical component of planetary scale EP flux (m^2/s^2) as 21 day running mean time vs. height plot. (a, b) averaged over Barents and Kara Sea (65°N-85°N and 30°E-90°E), (c,d) averaged over Pacific region (65°N-85°N and 150°E-120°W. (a,c) AFES NICE minus CNTL, (b,d) ERA-Interim low ice minus high ice period. Significance on 90% (dotted), 95% (dashed) and 99% (solid) level marked in black contours.

Figure 7: Decadal comparison of climatological quantities in ERA-Interim averaged over 65°N-85°N and 0°E-360°E as 21 day running mean time vs. height plot. (a,b) vertical component of planetary scale EP flux (m^2/s^2), (c,d) geopotential heights (gpm), (e,f) zonal wind anomalies (m/s) (a,c,e) low ice period minus 80s decade, (b,d,f) low ice period minus 90s decade. Significance on 90% (dotted), 95% (dashed) and 99% (solid) level marked in black contours.

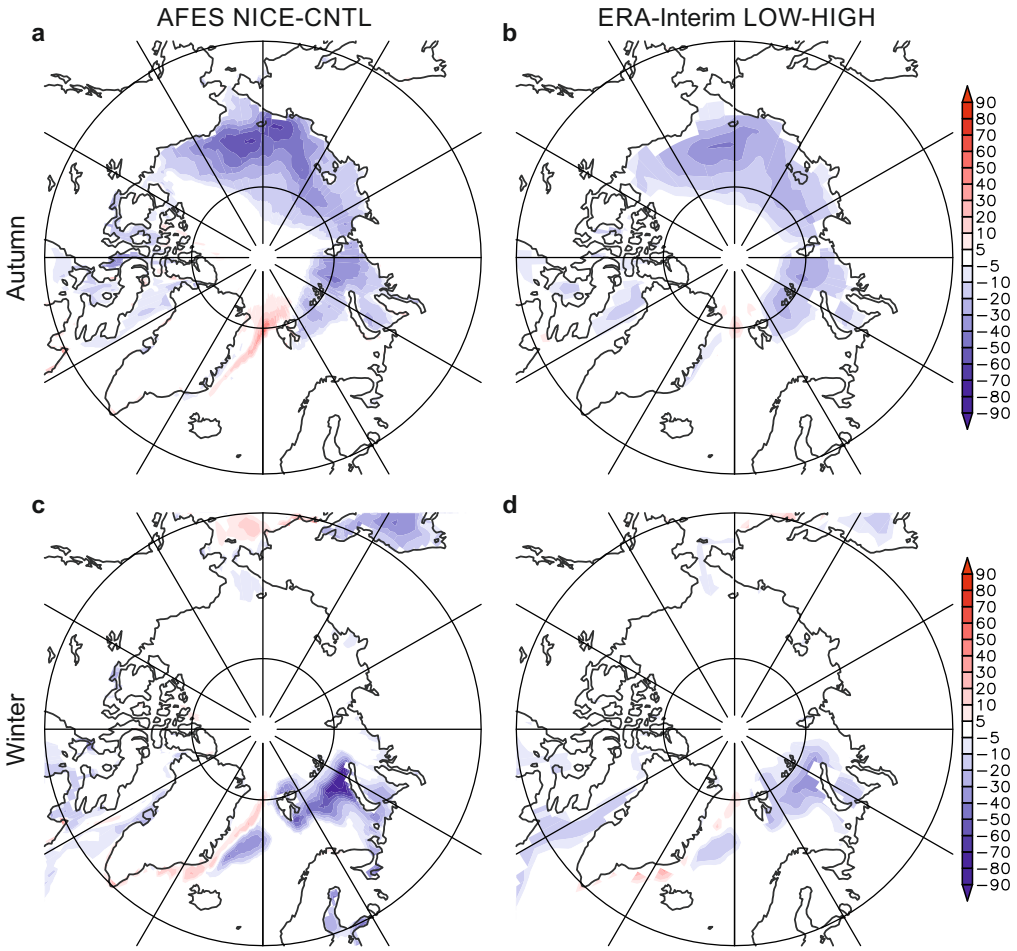
AFES NICE-CNTL
ERA-Interim LOW-HIGH
a
b
c
d
Autumn
Winter
90
80
70
60
50
40
30
20
10
5
−5
−10
−20
−30
−40
−50
−60
−70
−80
−90

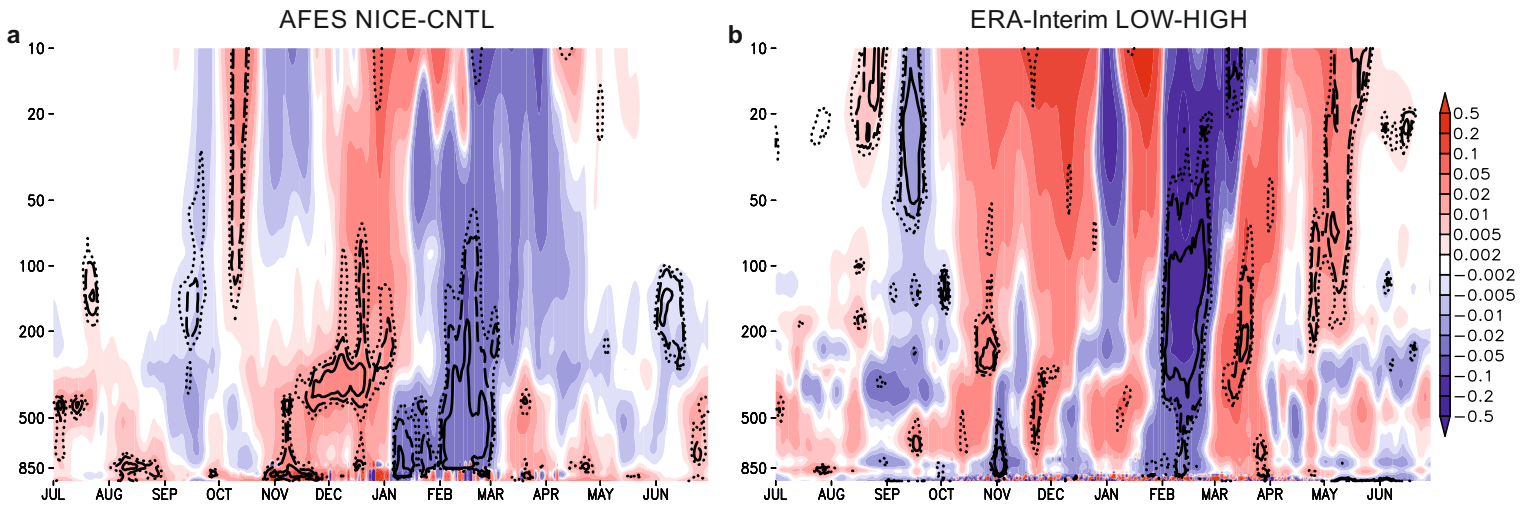
a
AFES NICE-CNTL
b
ERA-Interim LOW-HIGH
10
20
50
100
200
500
850
JUL
AUG
SEP
OCT
NOV
DEC
JAN
FEB
MAR
APR
MAY
JUN
0.5
0.2
0.1
0.05
0.02
0.01
0.005
0.002
−0.002
−0.005
−0.01
−0.02
−0.05
−0.1
−0.2
−0.5

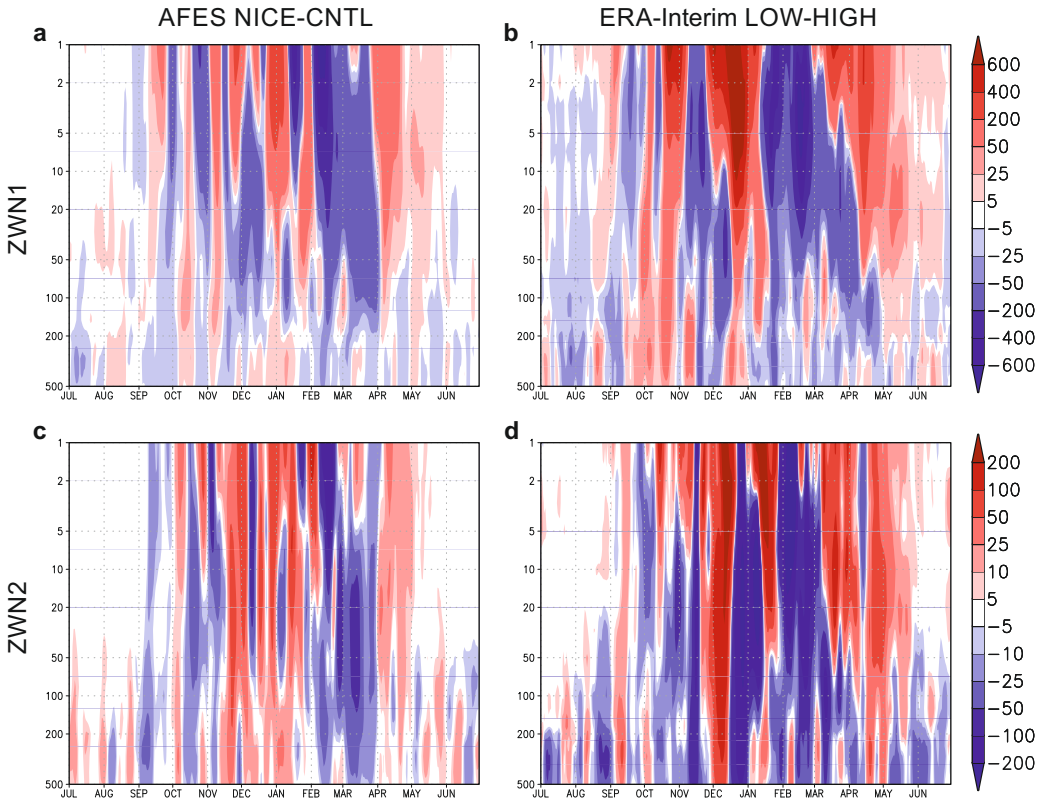
AFES NICE-CNTL
ERA-Interim LOW-HIGH
a
b
c
d
ZWN1
ZWN2
1
2
5
10
20
50
100
200
500
JUL
AUG
SEP
OCT
NOV
DEC
JAN
FEB
MAR
APR
MAY
JUN
600
400
200
50
25
5
−5
−25
−50
−200
−400
−600
200
100
50
25
10
5
−5
−10
−25
−50
−100
−200

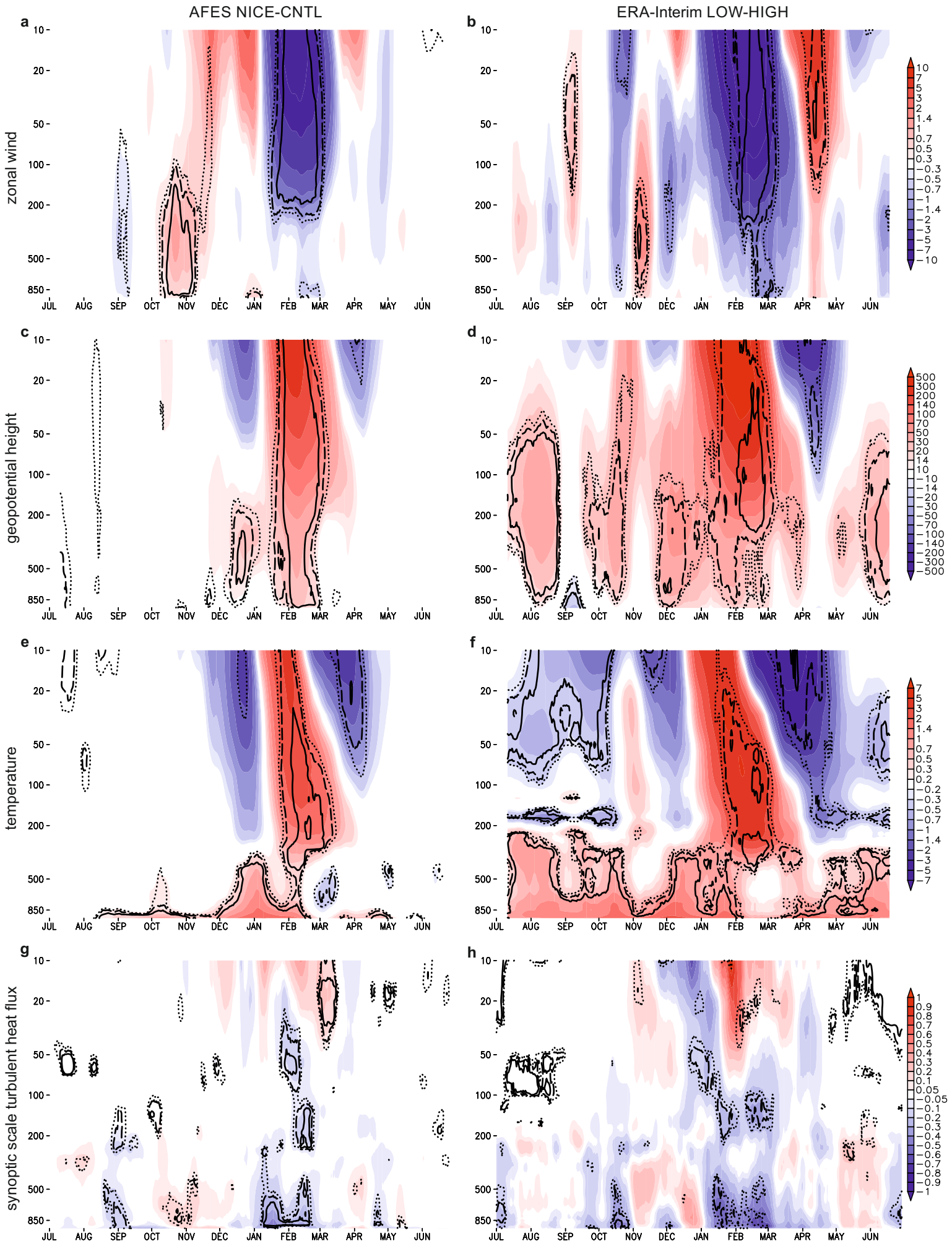
AFES NICE-CNTL
ERA-Interim LOW-HIGH
a
b
c
d
e
f
g
h
zonal wind
geopotential height
temperature
synoptic scale turbulent heat flux
10
20
50
100
200
500
850
JUL
AUG
SEP
OCT
NOV
DEC
JAN
FEB
MAR
APR
MAY
JUN
10 7 5 3 2 1.4 1 0.7 0.5 0.3 −0.3 −0.5 −0.7 −1 −1.4 −2 −3 −5 −7 −10
500 300 200 140 100 70 50 30 20 14 10 −10 −14 −20 −30 −50 −70 −100 −140 −200 −300 −500
7 5 3 2 1.4 1 0.7 0.5 0.3 0.2 −0.2 −0.3 −0.5 −0.7 −1 −1.4 −2 −3 −5 −7
1 0.9 0.8 0.7 0.6 0.5 0.4 0.3 0.2 0.1 0.05 −0.05 −0.1 −0.2 −0.3 −0.4 −0.5 −0.6 −0.7 −0.8 −0.9 −1

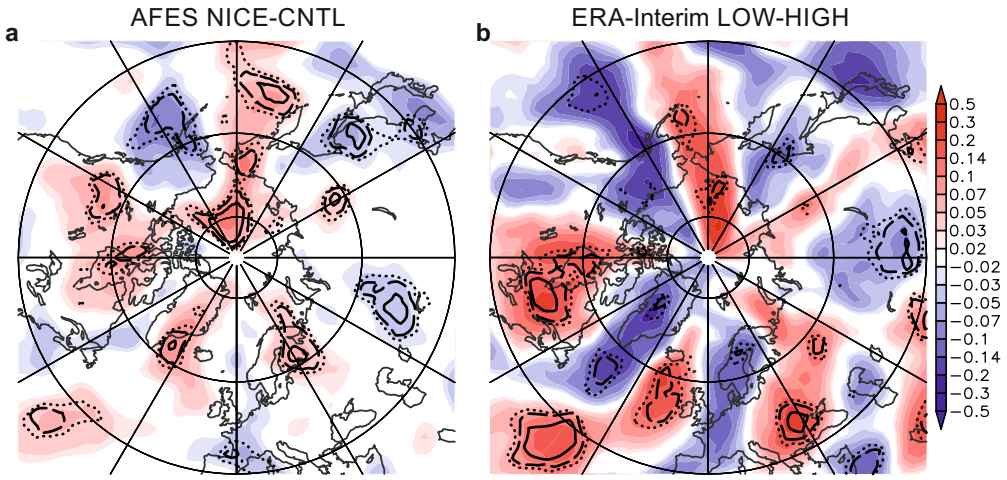
a
AFES NICE-CNTL
b
ERA-Interim LOW-HIGH
0.5
0.3
0.2
0.14
0.1
0.07
0.05
0.03
0.02
−0.02
−0.03
−0.05
−0.07
−0.1
−0.14
−0.2
−0.3
−0.5

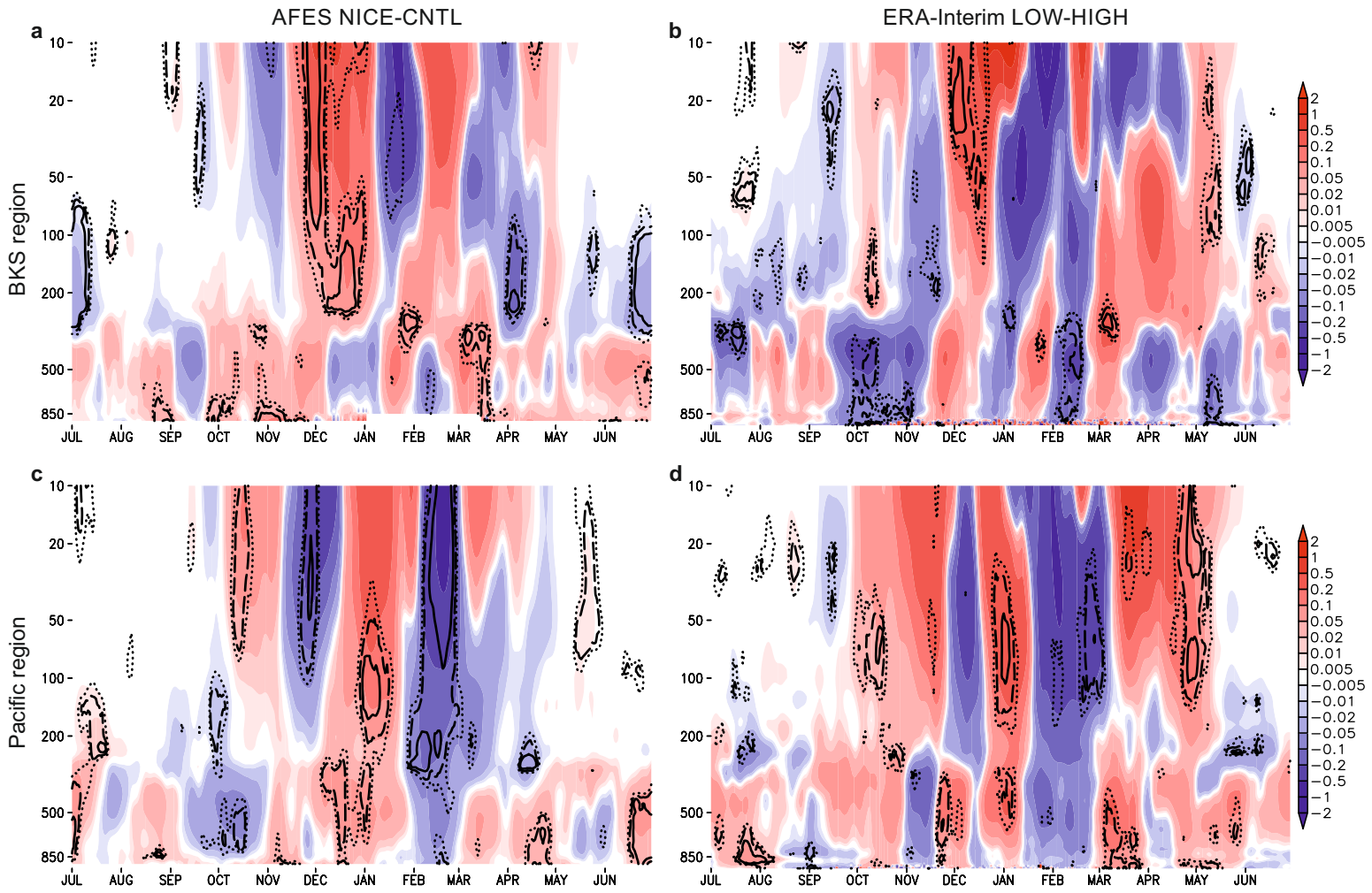
AFES NICE-CNTL
ERA-Interim LOW-HIGH
a
b
c
d
BKS region
Pacific region
10
20
50
100
200
500
850
JUL
AUG
SEP
OCT
NOV
DEC
JAN
FEB
MAR
APR
MAY
JUN
2
1
0.5
0.2
0.1
0.05
0.02
0.01
0.005
−0.005
−0.01
−0.02
−0.05
−0.1
−0.2
−0.5
−1
−2

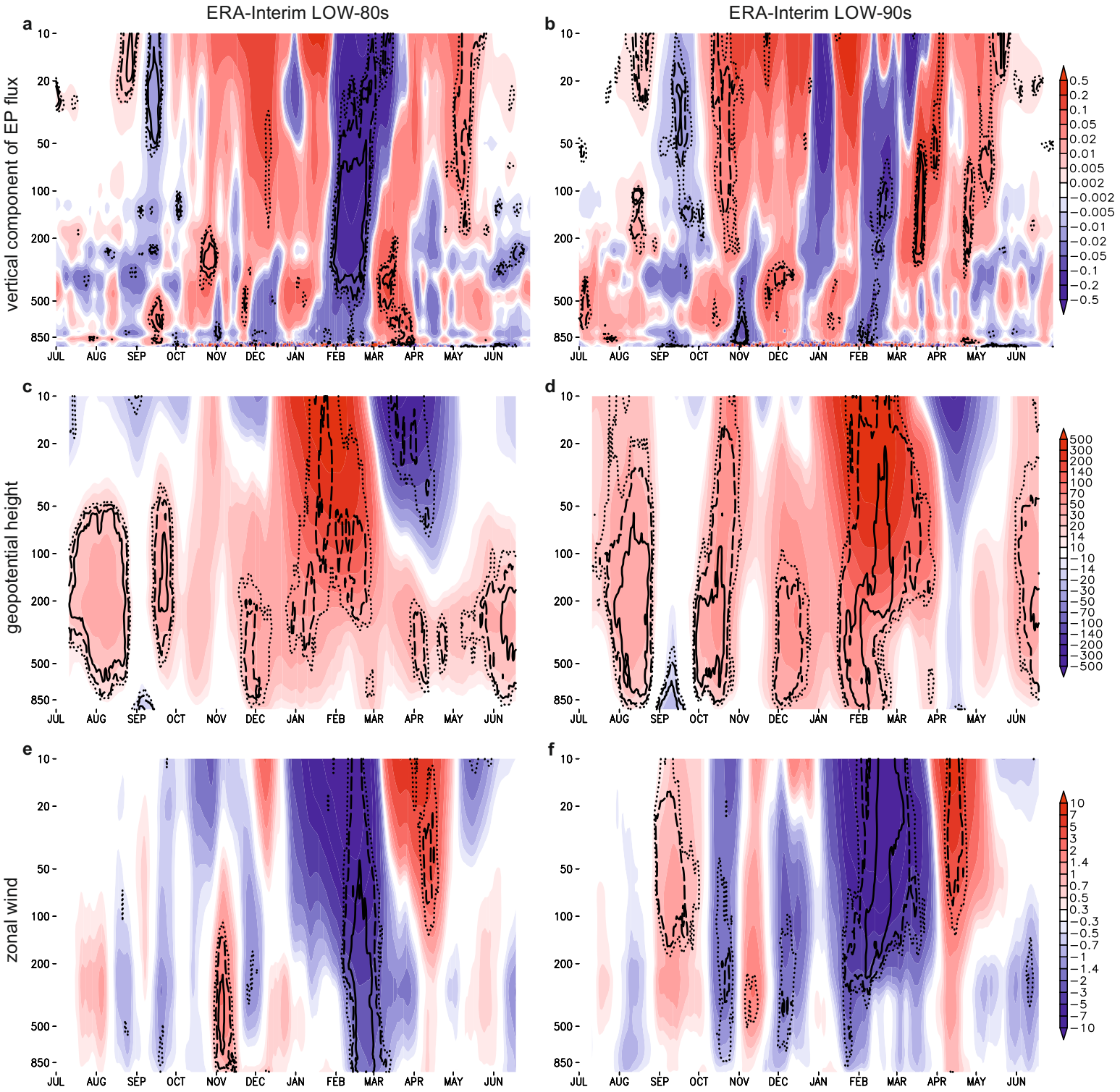
ERA-Interim LOW-80s
ERA-Interim LOW-90s
a
b
c
d
e
f
vertical component of EP flux
geopotential height
zonal wind
10
20
50
100
200
500
850
JUL
AUG
SEP
OCT
NOV
DEC
JAN
FEB
MAR
APR
MAY
JUN
0.5
0.2
0.1
0.05
0.02
0.01
0.005
0.002
−0.002
−0.005
−0.01
−0.02
−0.05
−0.1
−0.2
−0.5
500
300
200
140
100
70
50
30
20
14
10
−10
−14
−20
−30
−50
−70
−100
−140
−200
−300
−500
10
7
5
3
2
1.4
1
0.7
0.5
0.3
−0.3
−0.5
−0.7
−1
−1.4
−2
−3
−5
−7
−10